Journal of Biomedical Optics

BiomedicalOptics.SPIEDigitalLibrary.org

Simultaneous *en-face* imaging of multiple layers with multiple reference optical coherence tomography

Kai Neuhaus
Seán O'Gorman
Paul M. McNamara
Sergey Alexandrov
Josh Hogan
Carol Wilson
Martin J. Leahy

SPIE.

Kai Neuhaus, Seán O'Gorman, Paul M. McNamara, Sergey Alexandrov, Josh Hogan, Carol Wilson, Martin J. Leahy, "Simultaneous *en-face* imaging of multiple layers with multiple reference optical coherence tomography," *J. Biomed. Opt.* **22**(8), 086006 (2017), doi: 10.1117/1.JBO.22.8.086006.

Simultaneous *en-face* imaging of multiple layers with multiple reference optical coherence tomography

Kai Neuhaus,[a,*] Seán O'Gorman,[a] Paul M. McNamara,[a,b] Sergey Alexandrov,[a] Josh Hogan,[b] Carol Wilson,[b] and Martin J. Leahy[a,c,*]
[a]National University of Ireland, Tissue Optics and Microcirculation Imaging Facility, Galway, Ireland
[b]Compact Imaging, Inc., Mountain View, California, United States
[c]Royal College of Surgeons, Dublin, Ireland

Abstract. A technique based on multiple reference optical coherence tomography (MR-OCT) is proposed for simultaneous imaging at multiple depths. The technique has been validated by imaging a reference sample and a fingerprint *in-vivo*. The principle of scanning multiple selected layers is shown by imaging a partial fingerprint with $200 \times 200 \times 200$ voxels of $3 \times 3 \times 0.5$ mm size and obtaining an arbitrary amount of layers merely by digital processing. The spacing among the layers can be adjusted arbitrarily, and the SNR roll-off is shown for three different spacings. At a mirror scan frequency of 1 kHz and an A-line rate of 2 kHz, the acquisition time was 20 s for one volume. The results show the feasibility of the application of layer scanning MR-OCT that uses a partial mirror in the reference arm of the Michelson interferometer. The reduced scan range required for layer scanning allows even higher scan rates that are limited only by the voice coil design and the mass-spring system, e.g., mirror mass, spring constant, and damping. [DOI: 10.1117/1.JBO.22.8.086006]

Keywords: biomedical optics; image formation; optical systems; interference; engineering; coherent optical systems.

Paper 170340R received May 25, 2017; accepted for publication Jul. 24, 2017; published online Aug. 22, 2017.

1 Introduction

The motivation of multiple reference optical coherence tomography (MR-OCT) is to have a simple method of extending the scan range (SR) of a time-domain OCT (TD-OCT) with a minimal set of additional optical components and to still have the option of miniaturization.[1] The similarity of the MR-OCT technology to CD/DVD-ROM pick-up heads[2] allows the possibility of a rapid transfer into production with well-understood methods and production lines. Photonic-integrated circuits and wafer-level optics, including akinetic optical delay lines, will undoubtedly be the future as they have the highest integration density and will push the boundaries of miniaturization. However, integrated OCT systems[3] require a dedicated design process and the creation of suitable production methods before becoming commercially available with sufficient sensitivity. For portable continuous monitoring applications, the data volume that can be transmitted is often limited due to storage restrictions or the speed limitations of the wireless communication channels, in which case the moderate scan speed of MR-OCT may be a favorable factor.

In this report, a particular layer scanning method that allows the simultaneous formation of *en-face* imaging at regular depth intervals with minimal modification of an MR-OCT system is described.[2] This layer scanning MR-OCT (lsMR-OCT) can provide a low-cost platform for applications, including the imaging of *in-vivo* biological and biomedical specimens, such as human skin and the eye. The main limitation of lsMR-OCT is a compromise between A-line rate and scanning depth originating from the trade-off between the scan speed and the SR of the voice coil. At large axial scanning ranges, the orders will increasingly overlap, but the reduced A-line rate causes susceptibility to motion artifacts. At higher scanning rates, the layer thickness is reduced, limiting the visibility of structures in depth, although this could be improved with lsMR-OCT using a layer stepping similar to confocal microscopy. On the other hand, it has been previously shown that layered scanning can be used to extract sufficient information for evaluation without recording data over the full axial range[4] The A-line rate of 2 kHz is sufficient for biometric applications, and it is easy to adjust the depth range (set by the SR of the voice coil) and axial position of the layers [set by the separation of the scanning mirror (SM) and partial mirror (PM)] to increase the A-line rate if required. Hoeling et al.[5] reported a system with a resonant piezo stack with the ability to scan at 125 kHz with a scanning depth of 350 nm. If the same frequency would be applied to lsMR-OCT using, for example, only the first three orders of reflections, the axial SR for the third order would be three times that of the reference mirror SR. This will enable a confocal type OCT with three scanning layers at three regular parallel depth intervals or more if one wants to process more orders of reflections depending on the scattering properties of the sample.

A particular benefit of MR-OCT and lsMR-OCT is the availability of all interference signals from all depth layers in one sum-signal on one photodetector as opposed to other methods that require multiple detectors.[4,6] The benefits of lsMR-OCT over MR-OCT are A-line rates of currently 2 kHz and the ability to adjust the spacing between the selected *en-face* layers on demand, which has not been shown to be possible in other OCT systems. Such a selected layer imaging method allows

*Address all correspondence to: Kai Neuhaus, E-mail: k.neuhaus2@nuigalway.ie; Martin J. Leahy, E-mail: martin.leahy@nuigalway.ie

1083-3668/2017/$25.00 © 2017 SPIE

obtaining *en-face* images that have an exact position within the sample.

The sensitivity of the lsMR-OCT system is sufficient for extracting biometric markers, such as the fingerprint ridges, minutia, and subdermal features, such as sweat ducts, which can be used for the improved detection of fingerprint presentation attacks.[7] The most expensive component in the current research system is the superluminescent light-emitting diode, which has the potential to be reduced to a price comparable with that of laser diodes if produced in large quantities. Also, the photodetector unit can potentially be replaced with low-cost circuitry, and the digitizing system can be replaced with a suitable system on a chip.[8,9] Image processing can be supported by preprocessing units[10] or eventually completely on smartphones with sufficient processing power.[11]

To validate the lsMR-OCT method, images from two different commercial OCT systems were acquired. Imaging of the phantom (Fig. 5) was performed with a Telesto II system from Thorlabs ($\lambda_0 = 1300$ nm, BW = 170 nm, axial resolution in air 5.5 μm, maximum imaging depth 3.5 mm, maximum A-line rate 76 kHz, and superluminescent diode (SLED) power about 10 mW) while for the fingerprint imaging (Fig. 6), a Thorlabs OCS1300SS system ($\lambda_0 = 1300$ nm, BW = 100 nm, axial resolution in air 12 μm, maximum imaging depth 3.0 mm, maximum A-line rate 16 kHz, and SLED power about 10 mW) was used. All images were adjusted to an SR of 3×3 mm and 200×200 A-lines.

2 Materials and Setup

The optical layout of the investigated MR-OCT system to test the lsMR-OCT method is shown in Fig. 1. The PM selected had a splitting ratio of 80/20 (reflection/transmission), which was shown to produce a maximum amount of reflection without saturating the detector.

The focal length of lens L1 was coerced by the position of the PM. To achieve sufficient lateral resolution, it was necessary that the focal length of L2 was less than L1. The consequent dispersion effects were deemed as acceptable for the current setup and can be avoided by modifying the mount for the PM in future constructions.

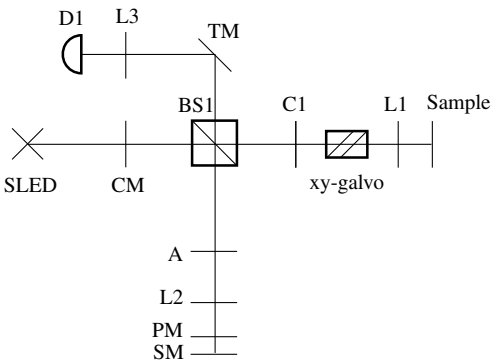

Fig. 1 The optical configuration of the lsMR-OCT system. The low coherent light source (SLED, DL-CS3207A) is a super-luminescent diode and fiber coupled over a collimator (CM). The reference arm consists of the SM, PM, a 75-mm achromatic lens doublet (L2), and attenuator (A) together with the beam splitter (BS1). The sample arm consists of a sample (e.g., *in-vivo* finger or mirror), a 30-mm lens doublet (L1), the xy-galvo for lateral scanning, and a blank (C1) to compensate for the path-length mismatch caused by the PM, L2, and A. The detector arm consists of a turning mirror (TM), a detector lens (L3), and the detector (D1, New Focus 2053).

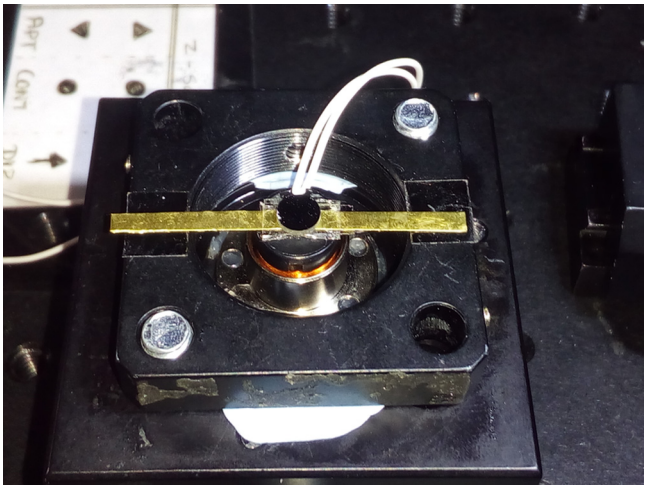

Fig. 2 Voice coil mounted on a bar-spring made of brass ($3 \times 0.3 \times 40$) mm. The resulting resonance frequency was close to 1 kHz.

For the axial scanning system, a mirror with a diameter of 5 mm was mounted on a bar spring (Fig. 2) and actuated by a voice coil. The engineering of the mirror scanning system was kept purposefully simple to investigate the impact of a low-cost assembling technique on the imaging performance. The resonance of the mass-spring system was determined to be 1 kHz, and an SR of the mirror was measured as 12 μm. Usually, for ordinary TD-OCT, such a small SR would be of little use; however, lsMR-OCT uses multiple reflections from the PM to obtain multiple imaging layers. For the purpose of imaging a fingertip *en-face,* 10 orders of reflections were processed with a depth of ~500 μm. For other applications, the imaging depth can easily be modified depending on the amount of processed orders of reflections.

The SM in conjunction with the PM does in theory generate an infinite amount of path length delays due to the light being reflected multiple times on the PM. Those multiple orders of reflections would mean an infinite amount of interference signals for infinite depth layers. The actual amount of visible interference signals is limited by the system SNR, the scattering properties of the sample material, and the chosen splitting ratio of the PM. During digital processing, the interference signals are separated by digital filtering and can be further selected depending on the application.

The interference signal for each SR or depth layer will have a distinct Doppler frequency f_D according to $f_D(N) = N \times f_0$, where N is the order of reflection and $f_0 = 2\bar{v}_M/\lambda_0$ is the fundamental interference frequency from the first direct reflection from the SM with an average linear mirror velocity $\bar{v}_M$ and a center wavelength of the light source λ_0.

The interference signals are separated by digital filtering and, after envelope detection, are assembled into one A-line buffer. The total reconstructed SR can be calculated[12] with $\mathrm{SR} = (\Delta z_M/2) \cdot (N+1) + D \cdot (N-1)$ using the SR Δz_M, the spacing D between the PM and the rest position of the SM, and a preselected amount of orders of reflections N to be processed.

The reconstructed signal response for a mirror in the sample arm at different depth positions is shown in Fig. 3. The width of the point spread function (PSF) was calculated by

$$l_c = \frac{2\ln(2)}{\pi}\frac{\lambda_0^2}{\Delta\lambda}. \quad (1)$$

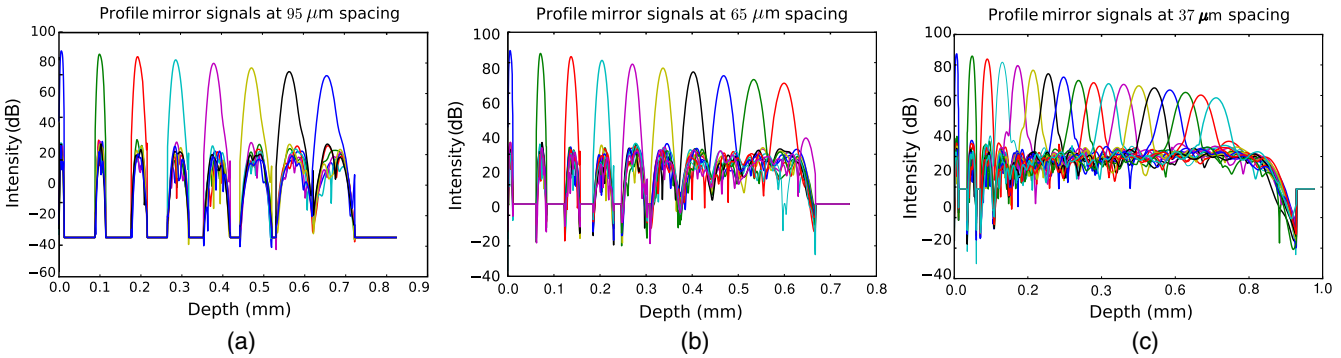

Fig. 3 Signal response (PSF) for three different spacings between PM and SM and each order of reflection. SP–PM spacing at (a) 95, (b) 65, and (c) 37 μm.

The light source used was a DL-CS3207A from Denselight with a center wavelength $\lambda_0 = 1310$ nm and a bandwidth of $\Delta\lambda = 65$ nm, which calculates to a full-width at half-mean (FWHM) of the PSF of $l_c = 13.5$ μm. The measured FWHM of the PSF was 20 μm, which is somewhat larger than the theoretical value but may be attributed to dispersion effects due to the mismatched lenses L1 and L2. The actual PSF at a depth close to the top surface (lower orders) is limited by the SR of the SM, which is 12 μm (Fig. 3). The thickness of the scanned layer increases for each order ($D \cdot N$). Furthermore, the FWHM of the PSF increases slightly for higher orders due to dispersion effects.

The SNR roll-off for the different spacings is shown in Fig. 4. The SNR reduces with increasing depth and higher orders, but if a sufficient amount of orders are closely spaced (Fig. 4), the increasing overlap of adjacent orders allows the reduction of the roll-off somewhat (see reduction of roll-off in Fig. 4 for 37 μm spacing at range 400 to 500 μm). In comparison, a reduced amount of orders with larger spacing will provide better SNR at deeper regions.

The theoretical signal for TD-OCT[13] on the detector is given by

$$I = I_R + I_S + 2\sqrt{I_R I_S} \cdot G(z) \cdot \cos(\omega t + \phi). \tag{2}$$

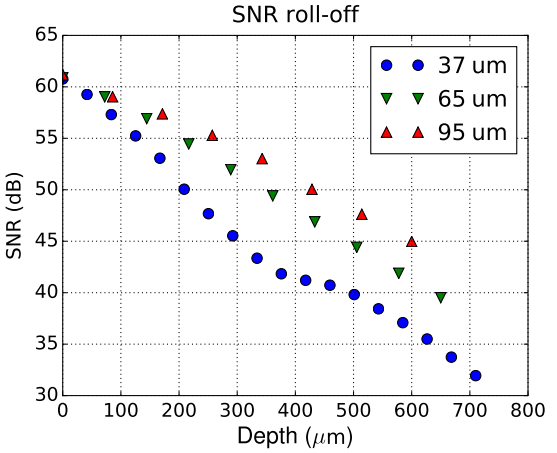

Fig. 4 The plot shows the intensity roll-off for all PM–SM spacings. Each data point corresponds to 1 order of reflection. A larger spacing has fewer orders and less roll-off. The SNR of higher orders of reflections is increasingly reduced due to the effect of the splitting ratio of the PM. A partial reduction of the SNR roll-off occurs at 400 μm to 500 μm when adjacent orders overlap (37 μm).

The parameters in the above equation are the intensity from the reference and sample arm I_R and I_S, the Gaussian shape $G(z)$ with a maximum of the Gaussian response at depth z with a frequency content $\cos(\omega t + \phi)$ and angular frequency ωt and phase ϕ.

For MR-OCT, Eq. (2) must be modified to

$$I = I_{PM} + \sum_N \{I_R(N) + I_S(N) + 2\sqrt{I_R(N) I_S(N)} \cdot G(N) \cdot \cos[\omega(N)t + \phi(N)]\}. \tag{3}$$

The modified equation [Eq. (3)] includes the total residual reflection from the PM, I_{PM}, and the summing of all generated interference signals. Although the amount of interference signals is in theory infinite, the actual amount of useful signals is limited due to the splitting ratio of the PM, scattering characteristics in the sample, and other optical losses and attenuations in the system.

It is not obvious that multiple reflections contribute with multiple powers originating from the reference arm $I_R(N)$, governed by the transmission T of the PM, which only interferes with a fractional power from the sample $I_S(N)$. This means that $I_S(N)$ describes the fraction of light that does create interference due to being in coherence with the fractional beam-power $I_R(N)$ at depth z_S. The reference arm power for each higher order of reflection can be calculated by $T^2(1-T)^{N-1}$ with T for the transmission ratio of the PM.

The signal characteristics for each higher order of reflection exhibit an increasing reduction of the width of the Gaussian envelope due to the increased SR "squeezed" into the buffer of the digitizer of constant length and time.[1] This squeezing effect of the Gaussian shape is based on the relative change of the time delay versus the coherence length and the resulting Gaussian characteristics.

Considering the relation of the coherence length l_C versus a time delay τ, the Gaussian[14] signal characteristics $G[\tau(N)]$ can be described by

$$l_c = c \int_0^\infty |G[\tau(N)]|^2 d\tau. \tag{4}$$

If $\tau(N) = [n_S z_S - z_M(N)]/c$ is the time delay introduced by the path-length difference between the sample reflector position $n_S z$ and the scan position of the SM z_M with the refractive index of the sample n_S and the speed of light c, then Eq. (4) allows the Gaussian term to be retrieved by considering the coherence

length versus the change of the time delay $\frac{l_c}{c\Delta\tau(N)} = G[\tau(N)]$, which effectively depends on the scan length $\Delta z_M(N)$. The scan distance Δz_M will increase in each mirror reflection due to the Doppler effect, and the light spectrum will shift to shorter wavelengths, effectively narrowing the Gaussian shape. The increased mirror SR can be expressed as $\Delta z_M(N) = N \cdot \Delta z_M$ or expressed as a time delay difference $\Delta\tau(N) = (n_S z_S - \Delta z_M \cdot N)$. Consequently, each higher order interference will have a distinct higher Doppler frequency with reduced Gaussian width related to the ordinal number of reflection N. To recover the actual corresponding axial SR after digitizing, each order of reflection is corrected by upsampling the buffer containing the filtered signal by a factor of N. Furthermore, the position of the Gaussian signal needs to be corrected within the sample buffer by calculating the depth position $z(N)$ based on the center of the SR $\Delta z_M/2$ using $z(N) = \Delta z_M/2 + D \cdot (N-1)$. This means that each order of reflection delivers an interference pattern at increasing depth intervals and each higher order increases in SR. The increase of the SR is a key feature of MR-OCT to allow larger imaging depths with a moderate or small SR of the SM. The increasing length of the scan regions causes increased overlaps between adjacent SRs, which could be useful for special signal analysis tasks.

For the investigated MR-OCT system, it was possible to detect up to 30 orders of reflections using a broadband mirror in the sample arm, while up to 20 orders have been found to be useful for imaging, which may vary depending on the adjusted spacing between PM and SM (see Fig. 4). The amount of orders providing interference is usually less due to dependence on the scattering and absorption properties of the sample. It was shown that it is possible to image up to 1-mm depth into a human finger tip *in-vivo*.[12]

3 Results

To validate the imaging capabilities of lsMR-OCT, a phantom was constructed made of a calibration grid from Thorlabs (R1L3S3P) with five layers of tape added to the rear site (Fig. 5), which was imaged with a Telesto II SD-OCT system.

It should be noted that the *in-vivo* scans of the fingerprint images (Fig. 6) were performed with an OCS1300-SS SD-OCT system. For the anticipated application to scan fingerprints, it is of interest to show the reproduction of images below a glass window that is compatible with frustrated total internal reflection fingerprint scanners.[15] The phantom, therefore, was prepared with five layers (thickness of each layer about 53 μm) of clear scotch tape and a final bottom paper layer to evaluate the sensitivity of structures below a slab of glass.

The tape layers in Fig. 5 are numbered from 1 to 5. Although the B-frame visibility (Fig. 5) is limited for lsMR-OCT, the anticipated *en-face* imaging mode shows a sensitivity sufficient for biometric identification. Due to the imperfections of the scanning system (Fig. 2), the axial pointing stability of the SM is reduced which, results in a strong reduction of sensitivity, reducing the visibility of structures within the higher orders of a B-frame. The *en-face* image reconstruction has a better contrast due to larger variations in intensity in the lateral direction. Particular material structures [Figs. 5(b) and 5(e)], such as circular patterns in the tape layers not visible otherwise were detected equally well with the lsMR-OCT system.

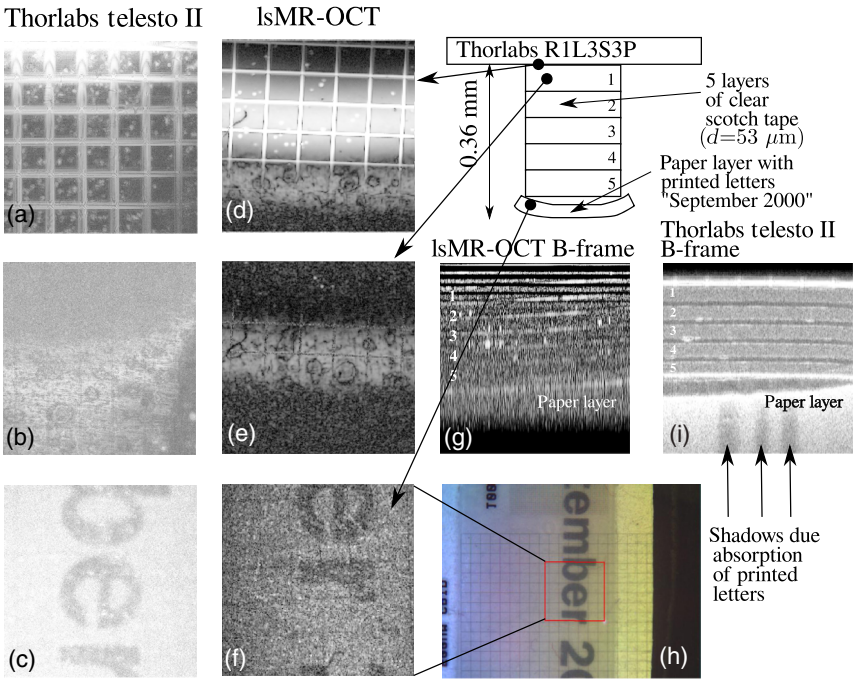

Fig. 5 The phantom was composed of a calibration grid slide (R1L3S3P) from Thorlabs and five layers of tape below the surface, including a paper layer at the bottom with printed letters (all images 200×200 pixel and 3×3 mm). The images (a), (b), and (c) show *en-face* structures from different layers taken with the Telesto II, and images (d), (e), (f) show according *en-face* images taken with lsMR-OCT. The images (g) and (i) show a B-frame taken with an lsMR-OCT (g) and taken with the Telesto II (i). A corresponding camera image of the printed letters is shown in (h). The top structure (a) and (d) show the grid and air bubbles in the glass–glue interface. The second layer (b) and (e) show structures in the tape material, and (c) and (f) show the bottom layer with printed letters "er."

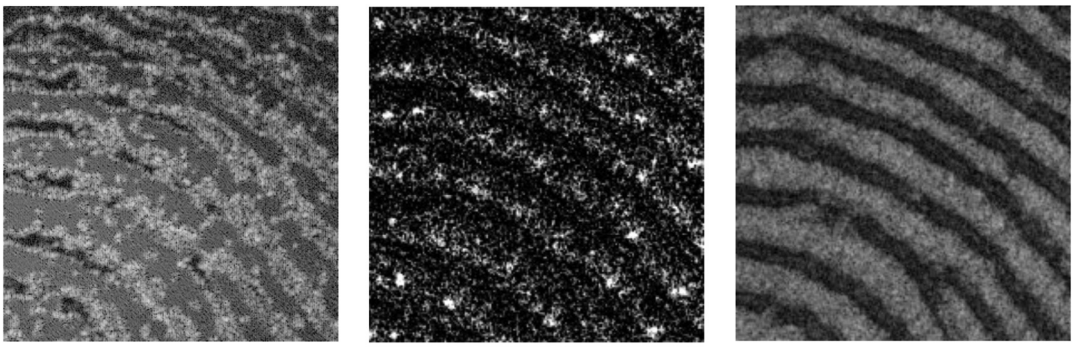

Fig. 6 *En-face* images of a fingertip below glass window taken with an SS-OCT system (OCS1300-SS) at three different depths. (a) Finger-glass interface, (b) sweat duct visibility (normalized, 0.2% pixel saturation), and (c) dermoepidermal junction.

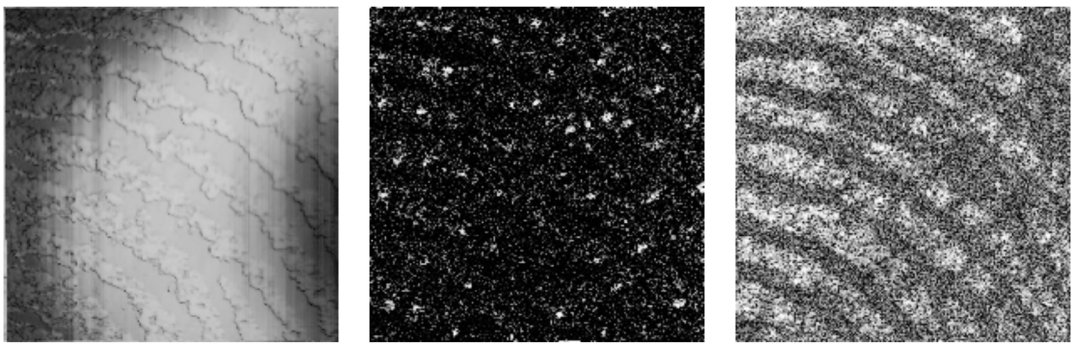

Fig. 7 *En-face* images of a fingertip below glass window taken with lsMR-OCT at three different depths. (a) Fingerprint structure finger–glass interface [$\Delta z(N = 1) = 12\ \mu$m], (b) sweat duct visibility (normalized, 0.2% pixel saturation), [$\Delta z(N = 1) = 60\ \mu$m], and (c) dermoepidermal junction (histogram equalized and normalized), [$\Delta z(N = 1) = 84\ \mu$m].

A human fingertip was scanned *in-vivo* with a Thorlabs OCS1300-SS SD-OCT system and lsMR-OCT, and the images are compared in Fig. 6 (OCS1300-SS) and Fig. 7 (lsMR-OCT). All images have a resolution of $200 \times 200 \times 200$ pixels and a 3×3 mm scan width. The images for the lsMR-OCT are shown for a PM–SM spacing of 37 μm. The fingertip structures for Figs. 6 and 7 were aligned to an optimal degree such that most or all features can be found in both images for comparison.

Images are shown for three different layers related to lsMR-OCT, and the depth was correspondingly used for the images taken with the OCS1300-SS system (the Telesto II was only used for the phantom imaging). The first layer corresponds to the top (finger-glass interface), the second layer is at a depth of about 150 μm, and the third layer is at about 300 μm located approximately at the dermoepidermal junction. The lsMR-OCT method can extract three features that can enhance the detection of presentation attacks, such as the structure of the superficial fingerprint, the structure of the dermoepidermal junction, and the location pattern of sweat ducts. For a thin *en-face* layer, the sweat duct visibility is limited due to a reduction of scattering events but is somewhat better for the OCS1300SS system. An estimation of the visibility was performed based on the area of the morphological features of the sweat ducts; for the OCS1300SS system, it was a mean area of 58 ± 37 pixels, and, for lsMR-OCT, it was 55 ± 28 pixels (larger area values correspond to a better contrast).

4 Conclusion

A technique, lsMR-OCT, for simultaneous formation of *en-face* and *in-vivo* imaging at various depths has been proposed; compared with other similar systems,[4,6] it can be constructed with a reduced set of components and provides additional imaging modalities not available otherwise. The lsMR-OCT system was investigated for *in-vivo* fingerprint identification applications using a light source with a wavelength of 1310 nm and an acquisition time of about 20 s for a scan volume of $200 \times 200 \times 200$ pixels. The obtained image quality is sufficient for identifying the surface ridge structure and comparing it with the subdermal structure, including the outline of the locations of the sweat ducts. If the relative geometric position of the sweat ducts is included as a biometric feature, another identification layer would be available using lsMR-OCT. Consequently, three biometric markers, such as ridge structure, matching subdermal boundary, and sweat duct pattern, would be available to improve biometric identification systems against presentation and spoofing attacks. The system was tested with a residual fingerprint on the glass surface, in which case no sweat ducts were visible and the subdermal boundary was missing. The proposed lsMR-OCT combines simple technologies into an application system that can help to improve current identification systems with a minimal effort and cost. Existing biometric databases can be used with lsMR-OCT as the enhanced detection of

additional biomarkers is an inherent feature of the technology. Upgrading databases with the added biomarkers can even further push the safety level of identification and the protection of a wide area of attacks related to fingerprint identification. The viability of lsMR-OCT can be found in the combination of a low-cost system with sufficient scanning speed. In particular, for a fingerprint scanning system, the skin is often stabilized on a glass window, reducing the demands on the scan rates.

Beyond the *in-vivo* fingerprint detection applications, the MR-OCT and lsMR-OCT each lends itself to the production of simple constructed systems at high volumes that can find application in remote monitoring or prescreening of biomarkers that do not require medical grade speed or sensitivity. Some unique features due to the multiple reflections may also be combined with other OCT technologies to create acquisition and detection mechanisms that have not been explored yet. The lsMR-OCT system exhibits a great flexibility for adapting to specific scanning solutions that compromise between high scan speed and scanning layer thickness. The PM could also be attached to a piezo-positioner for easy reconfiguration of the distance to the SM.

Using lsMR-OCT for ophthalmology monitoring, some parameters of the eye appear to be accessible by single point A-line measurements that do not require a full image, including the monitoring of the retinal layer thickness or turbidity of the vitreous body, in which case scanning of a few A-lines may be sufficient. Consequently, the applications for lsMR-OCT should be found not only for imaging, which typically requires higher scan rates, but also for simpler monitoring applications, such as detection of the heartbeat by monitoring bulk motion in tissue. The planned research to detect the flow of blood in capillaries in human skin is, therefore, a more challenging task due to motion artifacts impairing the signal quickly. On the other hand, if only a small volume is required, blood flow detection with a suitable scan rate can be possible. For *ex-vivo* applications, the demand for scan speed is even more relaxed, and lsMR-OCT can provide a viable low-cost and portable imaging system for field research. Occasionally, applications that can monitor material properties require inexpensive layer detection systems, and a scan rate in the kiloHertz range is sufficient.[16]

Disclosures

This work was supported by the National University of Ireland (NUI) Galway, the Galway University Foundation, the University of Limerick Foundation, the National Biophotonics Imaging Platform, Ireland, funded under the Higher Education Authority PRTLI Cycle 4, cofunded by the Irish Government and the European Union—Investing in your future, and Compact Imaging, Inc. All authors have a financial interest in Compact Imaging, Inc. The acquisition of the *in-vivo* samples do not affect any ethical, health, or privacy concerns and were performed according to the ethical regulations and safety standards of the NUI Galway.

References

1. M. Leahy et al., "Multiple reference optical coherence tomography (MR-OCT) system," *Proc. SPIE* **8580**, 85800L (2013).
2. R. I. Dsouza, "Towards low cost multiple reference optical coherence tomography for in vivo and NDT applications," Thesis, National University of Ireland, Galway (2016).
3. S. Schneider et al., "Optical coherence tomography system mass-producible on a silicon photonic chip," *Opt. Express* **24**, 1573–1586 (2016).
4. A. G. Podoleanu et al., "Simultaneous en-face imaging of two layers in the human retina by low-coherence reflectometry," *Opt. Lett.* **22**, 1039–1041 (1997).
5. B. M. Hoeling et al., "Phase modulation at 125 kHz in a Michelson interferometer using an inexpensive piezoelectric stack driven at resonance," *Rev. Sci. Instrum.* **72**, 1630–1633 (2001).
6. A. Meadway et al., "Multi-channel time domain spectroscopic optical coherence tomography system," *Proc. SPIE* **7139**, 713909 (2008).
7. C. Sousedik and C. Busch, "Presentation attack detection methods for fingerprint recognition systems: a survey," *IET Biom.* **3**(4), 219–233 (2014).
8. H.-S. Chen, B.-S. Song, and K. Bacrania, "A 14-b 20-Msamples/s CMOS pipelined ADC," *IEEE J. Solid-State Circuits* **36**, 997–1001 (2001).
9. Digi-Key Electronics, "AD9643-250EBZ Analog Devices Inc. Development Boards, Kits, Programmers|DigiKey," https://www.digikey.com/product-detail/en/analog-devices-inc/AD9643-250EBZ/AD9643-250EBZ-ND/2700345 (03 August 2017).
10. K. Guttag, "TMS320C8x family architecture and future roadmap," *Proc. SPIE* **2750**, 2 (1996).
11. K. C. Kim et al., "Smartphone-based portable ultrasound imaging system: a primary result," in *IEEE Int. Ultrasonics Symp. (IUS '13)*, pp. 2061–2063 (2013).
12. R. Dsouza et al., "Dermascope guided multiple reference optical coherence tomography," *Biomed. Opt. Express* **5**, 2870–2882 (2014).
13. M. E. Brezinski, *Optical Coherence Tomography: Principles and Applications*, Reed Elsevier, Cambridge, Massachusetts (2006).
14. J. M. Schmitt, A. Knüttel, and R. F. Bonner, "Measurement of optical properties of biological tissues by low-coherence reflectometry," *Appl. Opt.* **32**, 6032–6042 (1993).
15. H. C. Lee, R. Ramotowski, and R. E. Gaensslen, *Advances in Fingerprint Technology*, 2nd ed., CRC Press, Boca Raton, Florida (2001).
16. M.-T. Tsai et al., "Optical inspection of solar cells using phase-sensitive optical coherence tomography," *Sol. Energy Mater. Sol. Cells* **136**, 193–199 (2015).

Kai Neuhaus is a graduate student at the National University of Ireland, Galway, finalizing his PhD in biophotonics. He has industrial experience in software development and management, studied electrical engineering at the TU Chemnitz, Germany, and physics and instrumentation at the GMIT, Galway, Ireland. His current project is the optimization of MR-OCT for industrial applications, which includes the investigation and integration of optical systems and the optimization of data analysis systems.

Seán O'Gorman is a graduate student at the NUI, Galway. He specializes in multiple reference optical coherence tomography (MR-OCT) with a particular interest in angiography and liveness detection. His early research work is centered on cm OCT angiography of the nail fold plexus.

Paul M. McNamara received his PhD in biophotonics from the University of Limerick in 2013, specializing in tissue viability (TiVi) imaging and full-field optical coherence tomography. He is a postdoctoral researcher at the Tissue Optics and Microcirculation Imaging Group at NUI Galway and also head of Application Research Ireland for Compact Imaging Ireland, Ltd. His research interests include wearable devices and biophotonics applications in low-resource settings.

Sergey Alexandrov is a research scientist at the National University of Ireland (NUI), Galway. His main area of research is the development of new optical methods and tools, such as imaging and measuring techniques (holographic, interference, polarization, microscopy, OCT, spectral, etc.) for biomedical and other applications. His contributions have resulted in the creation of new optical methods and techniques for nondestructive testing, applications to different samples, including optical elements and systems, biomedical samples, and human beings *in vivo*.

Josh Hogan holds a doctorate in solid state physics from Ulster University. He is a founder and CTO of Compact Imaging, Inc. He holds over 50 patents, including several on compact imaging's

MR-OCT technology. Previously, he developed low-cost, small optoelectronic technologies, including DVD_RW optical storage systems, at HP Labs, Palo Alto, California.

Carol Wilson holds a doctorate in mechanical engineering from UC Berkeley. She is a cofounder and head of engineering at Compact Imaging, Inc. Previously, she developed low-cost small optoelectronics systems at HP Labs, Agilent, and IBM. She is named inventor on multiple patents and has won awards for her technical achievements.

Martin J. Leahy graduated with a DPhil in laser-based instrumentation for the measurement of blood flow and oxygenation from the University of Oxford in 1997. He is the head of the Tissue Optics and Microcirculation Imaging (TOMI) Group at NUI Galway. He is an adjunct professor at the Royal College of Surgeons, fellow of the Institute of Physics, Ireland, fellow of the Royal Academy of Medicine, Ireland, and fellow of SPIE.